

Available online at www.sciencedirect.com

ScienceDirect

Applied Ocean Research 28 (2006) 133-146

Applied Ocean Research

www.elsevier.com/locate/apor

Experimental and numerical evaluation of a typical dynamic positioning system

E.A. Tannuri*, H.M. Morishita

Department of Naval Architecture and Ocean Engineering, University of São Paulo, São Paulo, SP, Brazil Av. Prof. Mello Moraes, n. 2231, 05508-030, Cidade Universitária, São Paulo, SP, Brazil

Received 30 March 2005; received in revised form 20 May 2006; accepted 23 May 2006 Available online 26 September 2006

Abstract

A Dynamic Positioning System (DPS) is a complex control system composed of several algorithms, such as controllers, filters and optimal thrust allocation. The design, analysis and performance prediction of a DPS is normally done by a combination of static and dynamic numerical simulations and tank tests with a reduced model. After that, a long commissioning time is required to adjust control and filter parameters. This paper presents a computational dynamic simulator for DP systems, developed in a R&D project carried out at USP, called Numerical Offshore Tank (NOT). Some features of the simulator are the high speed calculation, thanks to a 120 processor cluster and the presentation of the results in a real time 3D-stereo visualization system. Furthermore, important parameters of the operation can be altered during the simulation, emulating a real DP console. It enables the simulation of most of a typical ship manoeuvering with DP especially those related to the offshore oil industry. Regarding offloading, the simulator can deal with multiple body systems taking into account the effects of risers, mooring lines and hawsers, if any. The Newtonian six-degrees-of-freedom model describes the dynamics of each vessel, in which validated models for environmental forces due to current, wind and waves are included. In order to pre-validate the simulator, a simplified experiment was set-up, composed of a reduced model of a DP tanker with 3 thrusters. Several experiments were carried out, and a detailed comparison with simulation results has shown very good agreement. Two loading conditions were considered: under the action of wind and current and the absence of both.

© 2006 Elsevier Ltd. All rights reserved.

Keywords: Dynamic positioning system; Kalman Filter; Offloading operation

1. Introduction

Dynamic Positioning Systems (DPS) are defined as a set of components used to keep a floating vessel in a specific position or pre-defined path through the action of propellers. DPS include position and heading measurement systems, a set of control algorithms, and propellers. Several offshore operations are carried out using DPS, such as drilling, pipelaying, offloading, and diving support.

Numerical and experimental tools must be used to design, analyze and predict the performance of a DPS before commissioning it. A DPS is a very complex system that integrates several components, and the overall reliability is a fundamental issue in all offshore operations. The motion

E-mail address: eduat@usp.br (E.A. Tannuri).

of a ship is affected by uncertain environmental forces with a broad frequency spectrum, which imposes the necessity of including complex control and filtering algorithms into the DPS. Furthermore, the dynamics of a ship is modeled by a highly nonlinear equation that makes the design of such algorithms an even harder task.

This paper describes recent facilities developed at the University of São Paulo to deal with DPS, namely a computational dynamic simulator and a model scale test system in a laboratory tank. In fact, the purpose of the simulator is to analyse the performance of the DPS in a scenario of offshore oil industry. Thus, it enables the simulation of typical DP operations, such as station keeping, path following, and assisted offloading. Each vessel is modeled by a six-degrees-of-freedom nonlinear equation in which validated models for environmental forces (current, wind and waves), main DPS algorithms, and a complete dynamic description of the propulsion system are included. If offloading operation from an anchored FPSO (Floating, Production, Storage and Offloading)

^{*} Corresponding author at: Department of Naval Architecture and Ocean Engineering, University of São Paulo, São Paulo, SP, Brazil. Tel.: +55 11 3091 5350 r.266.

is under consideration, the effects of risers, mooring lines and hawsers can be taken into account. The simulation is executed in a 120 processor cluster, and the results can be analyzed in real-time during the simulation, using a 3D-stereo visualization system [1].

In order to pre-validate the simulator, a simplified experiment was set-up, composed of a reduced model of a DP tanker with 3 thrusters. The measurement system is based on a computational vision positioning system. Control software contains the same DP algorithms used in the simulator, and is executed in an external computer which sends commands to the model by means of a wireless radio communication system. Basic wind and current generators were also constructed.

The DP algorithms used in the simulator and in the experimental set-up try to emulate commercial DP systems. An Extended Kalman Filter is then applied cascaded with a Proportional-Derivative controller and an optimal thrust allocation algorithm.

Early Dynamic Positioning Systems were based on three term PID control with a notch filter in order to avoid using the thruster to counteract high frequency motion due to waves. However, the controller based on the classical control theory exhibits phase lag that causes performance loss. In order to try to solve this problem, DPS with Extended Kalman Filter was proposed in the 1970s and nowadays it is the standard for all commercial DPS [2]. Several reasons explain the wide application of EKF in DP systems. The EKF reduces the phase lag caused by the filtering process, compared to conventional low-pass or notch filters [3], as it incorporates a model of the system, enabling it to make predictions about the motions. The reduction of phase lag results in a better performance and smaller control power. Furthermore, the EKF allows the utilization of several redundant sensors, and performs optimal estimation of the position and heading based on their information. This feature is important for DPS, since reliability and security are key issues for such systems. Finally, the EKF also predicts the environmental forces acting on the vessel, which is important information for the operators and may be used in the controller instead of an integral action [4].

It must be emphasized, however, that the EKF technique presents several drawbacks. There is a large number of tuning parameters which require a time-consuming tuning procedure. Furthermore, it requires the use of a gain-scheduling technique, since the model is linearized about approximately 36 yaw angles due to the kinematics equations of motions [5]. As an alternative to the EKF approach, a novel nonlinear observer was recently proposed by [5] with excellent results in both simulations and sea trials. Such an observer does not present the problems of EKF, and is based on passivity property of the ship dynamics. However, since the purpose of the simulator is to emulate real DP Systems, the simulator and experiment still adopt the EKF solution.

The control algorithm itself calculates thrust forces and moments based on low-frequency motion estimates. Modern commercial systems still employ simple PD algorithms. The integral action is given by direct compensation of

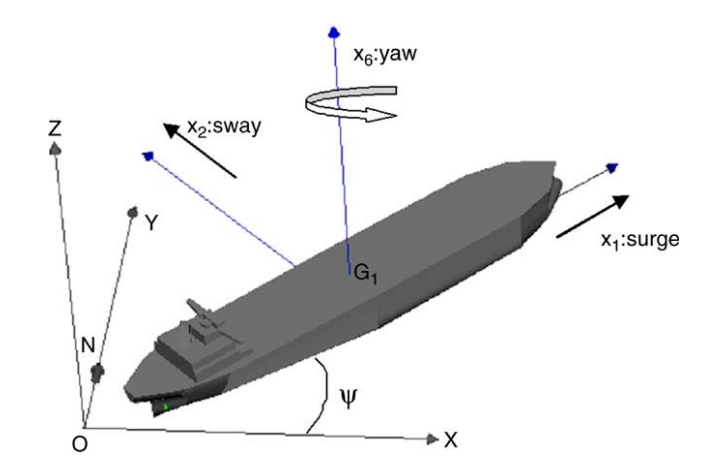


Fig. 1. Coordinate systems.

environmental forces, which are also estimated by the Kalman filter, as will be shown in the next section.

In the present paper, the basic modeling of the system is presented in Section 2. The numerical simulator and all DP algorithms are detailed in Section 3. The experimental set-up is described in Section 4, with comparisons between simulation and experimental results presented in Section 5. Finally, Section 6 presents the conclusions.

2. System modeling

For the purpose of DP Systems, only the horizontal motions of the ship need to be considered and the mathematical model can be built applying mechanical laws. The low-frequency motion of the system can be conveniently expressed in two orthogonal reference systems, one being the Earth fixed (OXYZ) and the other ($Gx_1x_2x_3$) a non-inertial reference frame fixed in the vessel (see Fig. 1). The origin of the latter frame is the intersection of the mid-ship section with the longitudinal plane of symmetry of the ship, and it is assumed to be coincident with the center of the ship mass. Additionally, the axes of reference frame are assumed to be coincident with the principal axes of inertia of the vessel. Bearing in mind those assumptions, the resulting equations of low-frequency motions related to non-inertial reference frame are:

$$(M + M_{11})\ddot{x}_{1} - (M + M_{22})\dot{x}_{2}\dot{x}_{6} - M_{26}\dot{x}_{6}^{2} + C_{11}\dot{x}_{1}$$

$$= F_{1E} + F_{1T} + F_{1M};$$

$$(M + M_{22})\ddot{x}_{2} + M_{26}\ddot{x}_{6} + (M + M_{11})\dot{x}_{1}\dot{x}_{6} + C_{22}\dot{x}_{2}$$

$$= F_{2E} + F_{2T} + F_{2M};$$

$$(I_{Z} + M_{66})\ddot{x}_{6} + M_{26}\ddot{x}_{2} + M_{26}\dot{x}_{1}\dot{x}_{6} + C_{66}\dot{x}_{6}$$

$$= F_{6E} + F_{6T} + F_{6M}.$$

$$(1)$$

where I_z is the moment of inertia about the vertical axis, M is the mass of the vessel, C_{ij} are damping coefficients, M_{ij} are added mass terms, F_{1E} , F_{2E} , F_{6E} are surge, sway and yaw environmental loads (current, wind and waves), F_{1T} , F_{2T} , F_{6T} are forces and moment delivered by the propulsion system and F_{1M} , F_{2M} , F_{6M} are forces and moment due to risers, mooring lines and hawsers, if any. The variables \dot{x}_1 and \dot{x}_2 are surge and sway low-frequency velocities and \dot{x}_6 is the yaw rate.

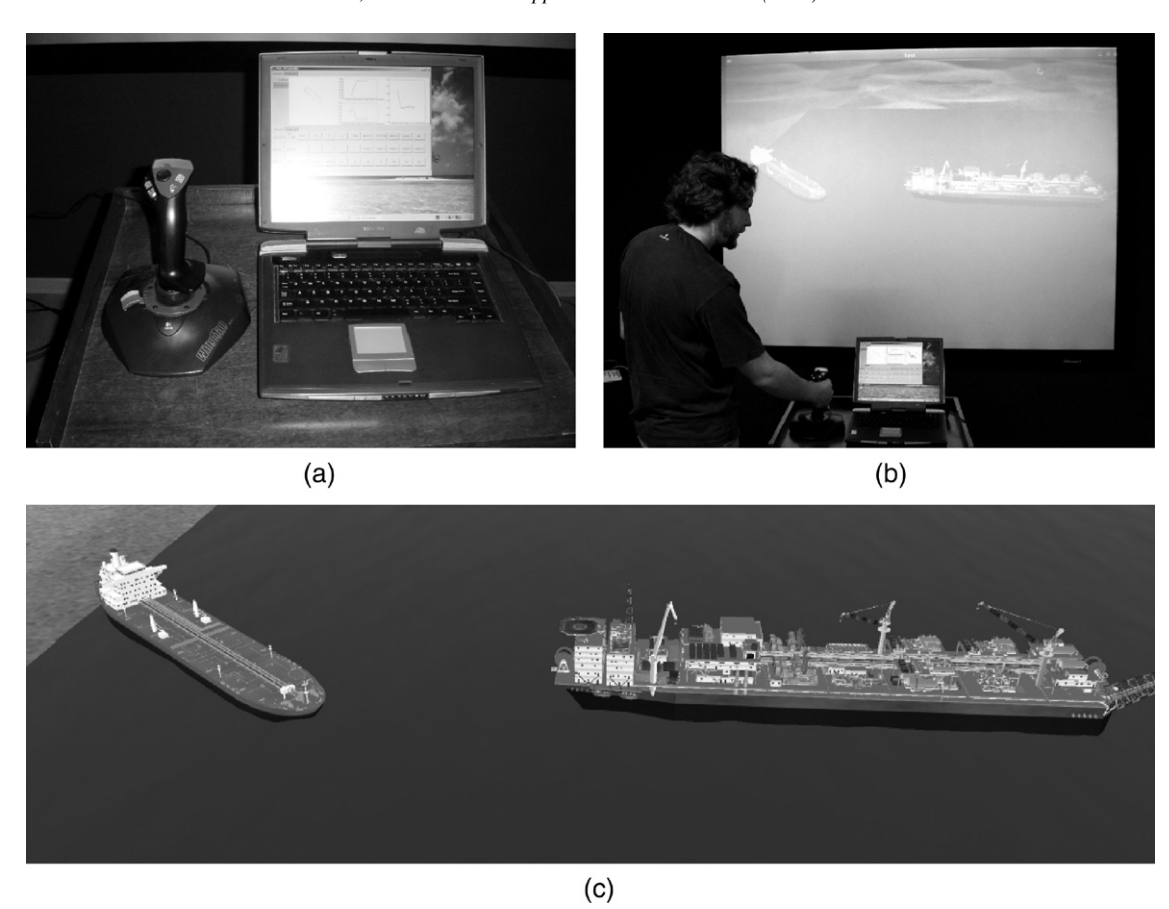


Fig. 2. NOT — (a) DP console emulator with joystick; (b) simulation being conducted; (c) 3D visualization.

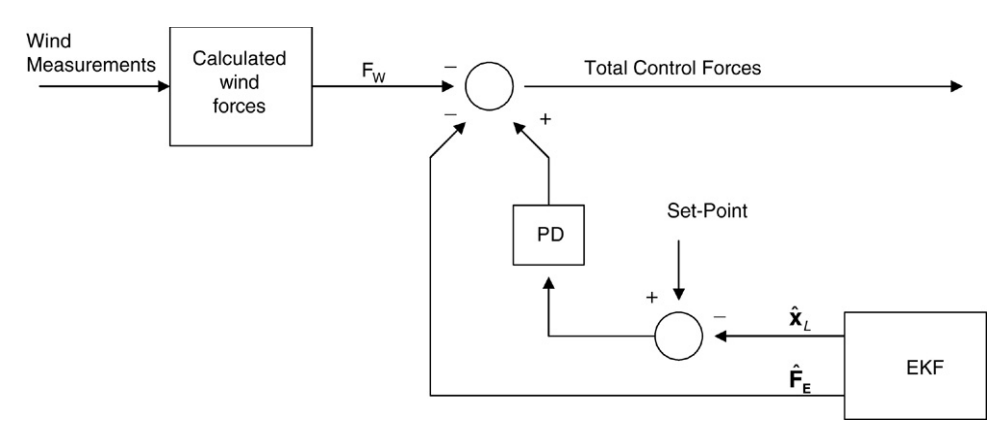


Fig. 3. EKF and controller block diagram.

The position and heading of the vessel related to the Earthfixed co-ordinate system are obtained from the following equation:

$$\begin{pmatrix} \dot{X}_L \\ \dot{Y}_L \\ \dot{\psi}_L \end{pmatrix} = T(\psi) \begin{pmatrix} \dot{x}_1 \\ \dot{x}_2 \\ \dot{x}_6 \end{pmatrix},$$
with $T(\psi_L) = \begin{pmatrix} \cos(\psi_L) & -\sin(\psi_L) & 0 \\ \sin(\psi_L) & \cos(\psi_L) & 0 \\ 0 & 0 & 1 \end{pmatrix}.$ (2)

Current induced forces are determined via a heuristic model based on a low aspect ratio wing theory with

experimental validation [6]. Wind forces are calculated employing coefficients suggested by [7] and wind gusts are also considered. Wave drift forces are evaluated using the hull drift coefficients worked out by means of a standard second-order potential flow analysis performed by computer software (Wamit). The interaction between current and waves (wave-drift damping) is also taken into account [8].

Wave-frequency (first-order) motions (X_H, Y_H, ψ_H) are evaluated by means of transfer functions related to the wave height, namely Response Amplitude Operators (RAOs), and are obtained via numerical methods modeling the potential flow around the hull. Such an approach is grounded in the

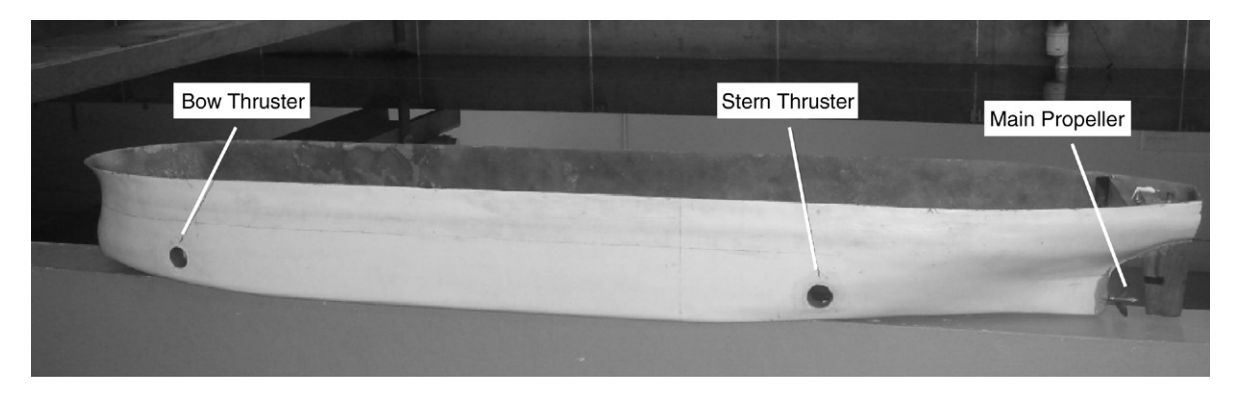


Fig. 4. Tanker reduced model.

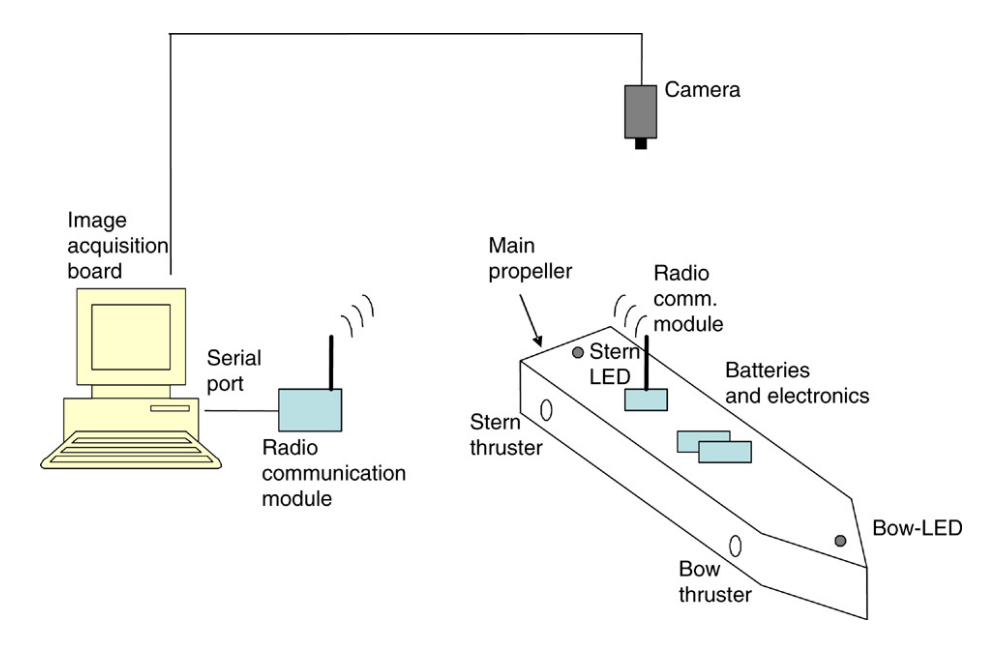


Fig. 5. Set-up of the DP experiment.

assumption of the linear response of wave-frequency motions and in the uncoupling between wave-frequency and low-frequency motions. Therefore, the real position of the vessel (X, Y, ψ) can be given by:

$$\begin{pmatrix} X \\ Y \\ \psi \end{pmatrix} = \begin{pmatrix} X_L \\ Y_L \\ \psi_L \end{pmatrix} + \begin{pmatrix} X_H \\ Y_H \\ \psi_H \end{pmatrix}. \tag{3}$$

3. Numerical simulator

As already mentioned, the Numerical Offshore Tank (NOT) is an advanced offshore system simulator. Furthermore, it is equipped with a console that emulates a real DP system, including a joystick for the fully-manual and semi-automatic control modes (see Fig. 2). Propellers can be disabled or enabled during the simulation, and one can evaluate the consequences of simple or multiple failures.

Several experimental and numerical validations have been conducted with NOT and its desktop version (called Dynasim).

These are considered important tools for design and analysis in the Brazilian oil industry [1,9,10].

A low-pass wave filter is employed to separate highfrequency components (excited by waves) from measurement signals. Such a decomposition must be performed because the DPS must only control low-frequency motion, since high-frequency motion would require enormous power to be attenuated and could cause extra tear and wear on propellers. Furthermore, an optimization algorithm, called thrust allocation, must be used to distribute control forces among thrusters. It guarantees minimum power consumption to generate the required total forces and moment, positioning the vessel. Finally, a control algorithm uses the filtered motion measurements to calculate such required forces and moment. Normally, a wind feedforward control is also included, enabling estimation of wind load action on the vessel (based on wind sensor measurements) and compensation by means of propellers.

In order to address the performance of commercial DPS, a conventional control algorithm was implemented in the

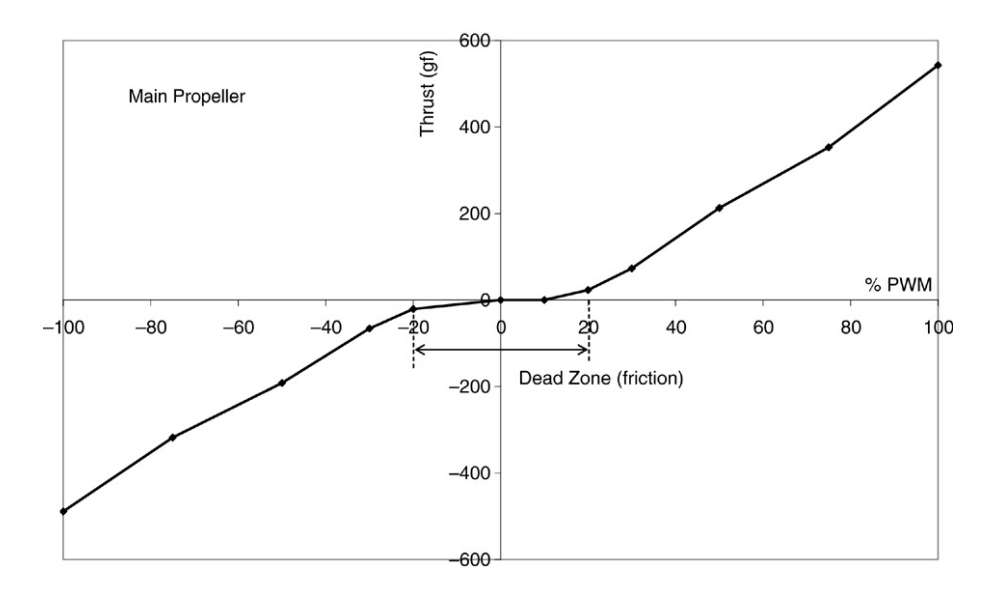


Fig. 6. Main propeller: thrust and command relation.

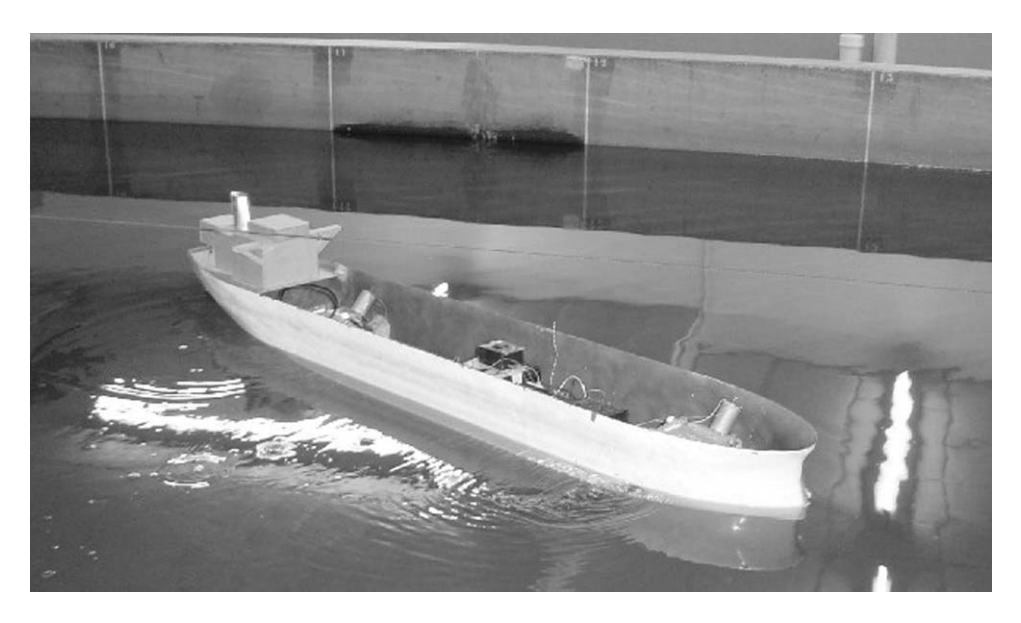


Fig. 7. Experiment in ballasted condition.

simulator, namely a 3-axis uncoupled PD controller, coupled to a feedforward wind compensator. Furthermore, an Extended Kalman Filter (EKF) was used as the wave filter. Such a filter also predicts the non-measured environmental forces, which can be used by the controller. The EKF estimator is widely used in commercial systems. Finally, a thrust allocation algorithm, based on a pseudo-inverse matrix technique, was implemented with extra features that are normally employed in real DPS.

Three DP operation modes were considered in the simulator. The first mode was the conventional station-keeping mode, in which the desired position and heading (set-point) were fixed. It is extensively used in drilling operations. Furthermore, a path-following mode was also considered, with a time-varying set-point, commonly used in pipe-laying operations. Finally, offloading operations require special control strategies, which were also implemented in NOT. Such operations may present

quite an interesting dynamic behavior and equilibria maps, as shown in [11].

The simulator also includes models for commonly used propellers, taking into account their characteristic curves, being able to estimate real power consumption and delivered thrust. It also evaluates the time delay between command and propeller response, caused by inertia.

In the following, each feature of the simulator related to DPS simulation is described in detail.

3.1. Extended Kalman Filter (EKF)

With X_L and Y_L being the position of the central point of the vessel, ψ_L the heading angle, the low frequency motion can be described by:

$$\dot{x}_{L} = A_{L}^{6 \times 6} x_{L} + A_{EL}^{6 \times 3} F_{E} + E_{L}^{6 \times 3} \omega_{L} + B_{L}^{6 \times 3} F_{T} \tag{4}$$



Fig. 8. Condition: (left) only current; (right) current + wind.

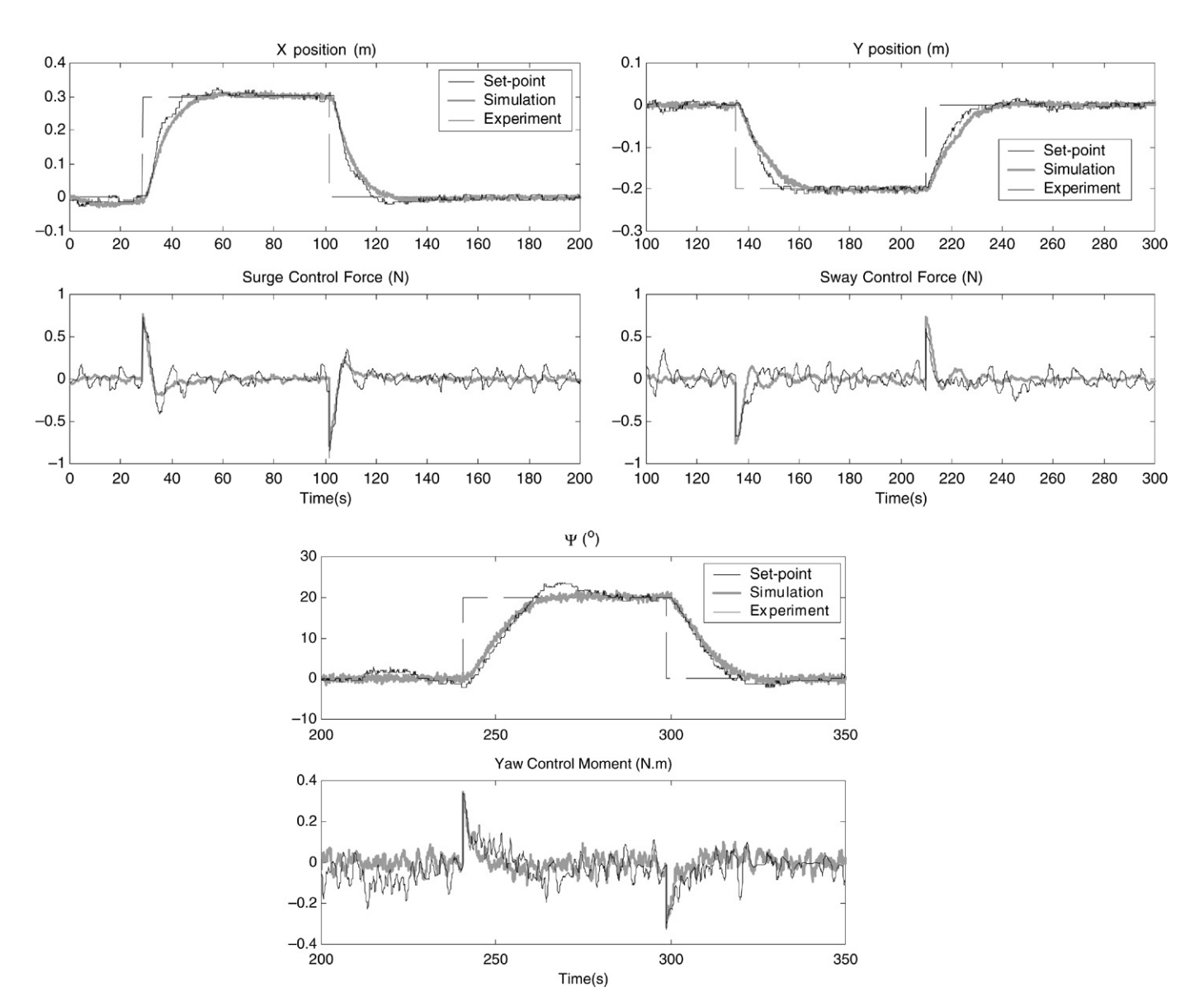


Fig. 9. Full condition, no environmental action.

where

$$\begin{split} \mathbf{A}_{\mathbf{L}}^{6\times6} &= \begin{pmatrix} \mathbf{0}_{3\times3} & \mathbf{T}(\psi_L) \\ \mathbf{0}_{3\times3} & -\mathbf{M}^{-1}\mathbf{C}_{3\times3} \end{pmatrix}; \\ \mathbf{A}_{\mathbf{EL}}^{6\times3} &= \mathbf{B}_{\mathbf{L}}^{6\times3} = \mathbf{E}_{\mathbf{L}}^{6\times3} = \begin{pmatrix} \mathbf{0}_{3\times3} \\ \mathbf{M}^{-1} \end{pmatrix}; \end{split}$$

 $\mathbf{x_L} = \begin{pmatrix} X_L & Y_L & \psi_L & \dot{x}_1 & \dot{x}_2 & \dot{x}_6 \end{pmatrix}^T$, $\mathbf{F_T}$ are thruster forces and moment vector, $\mathbf{F_E}$ are low frequency external forces and moment vector (including environmental and mooring forces), \mathbf{M} is the mass matrix of a vessel and \mathbf{C} is a damping matrix;. $\boldsymbol{\omega_L}$ is a 3×1 vector containing zero-mean Gaussian white noise

processes with covariance matrix \mathbf{Q}_L ($\boldsymbol{\omega}_L \sim N(0, \mathbf{Q}_L)$). The subscript \mathbf{L} is related to low frequency motion.

The forces F_E are slowly varying unknown variables, and can be modeled by:

$$\dot{\mathbf{F}}_{\mathbf{E}} = \mathbf{\omega}_{\mathbf{FL}} \tag{5}$$

where ω_{FL} is a 3 × 1 vector containing zero-mean Gaussian white noise processes with covariance matrix \mathbf{Q}_{FL} ($\omega_{FL} \sim N(0, \mathbf{Q}_{FL})$).

Finally, high frequency motions can be modeled by [2]:

$$\dot{\mathbf{x}}_{\mathbf{H}} = \mathbf{A}_{\mathbf{H}}^{6 \times 6} \mathbf{x}_{\mathbf{H}} + \mathbf{E}_{\mathbf{H}}^{6 \times 3} \boldsymbol{\omega}_{\mathbf{H}} \tag{6}$$

with

$$\mathbf{A}_{\mathbf{H}}^{6\times6} = \begin{pmatrix} \mathbf{0}_{3\times3} & \mathbf{I}_{3\times3} \\ -\omega_0^2\mathbf{I}_{3\times3} & -2\zeta\omega_0\mathbf{I}_{3\times3} \end{pmatrix}; \qquad \mathbf{E}_{\mathbf{H}}^{6\times3} = \begin{pmatrix} \mathbf{0}_{3\times3} \\ \mathbf{I}_{3\times3} \end{pmatrix}$$

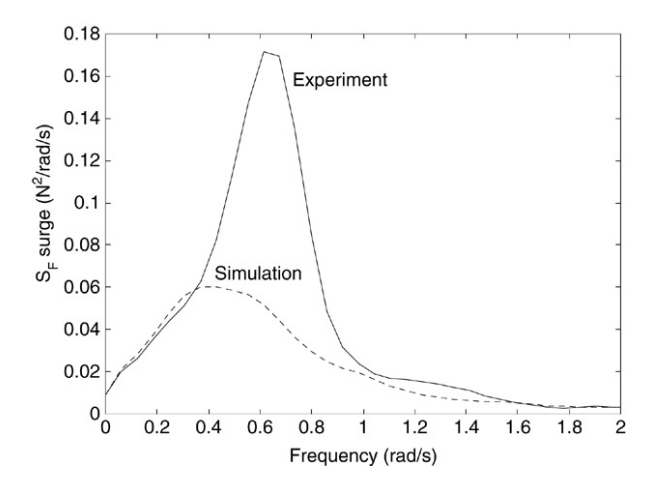


Fig. 10. Spectra of surge control force.

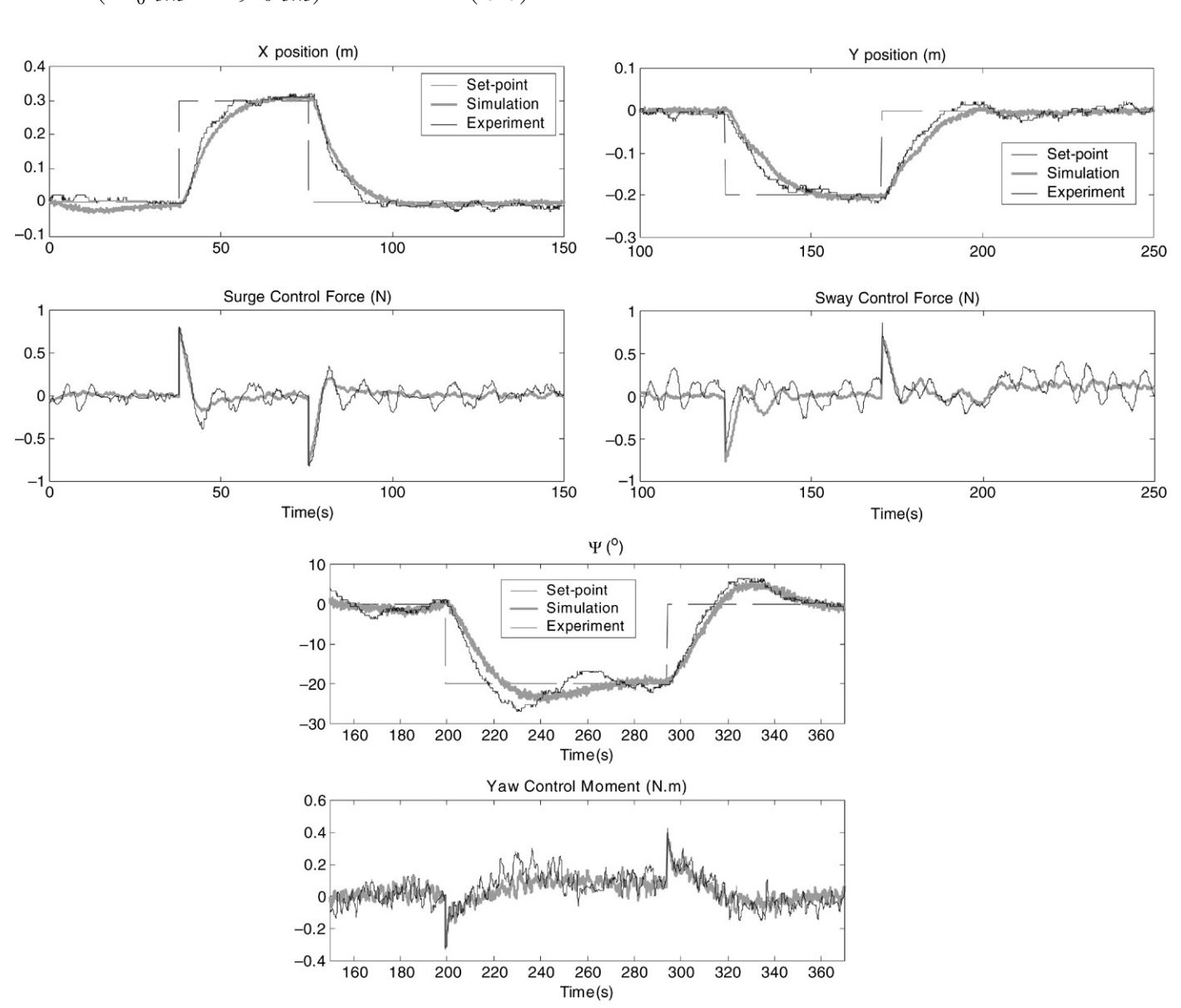


Fig. 11. Full condition, current action.

where

$$\mathbf{x}_H = \left(\int X_H \mathrm{d}t \quad \int Y_H \mathrm{d}t \quad \int \psi_H \mathrm{d}t \quad X_H \quad Y_H \quad \psi_H \right)^T,$$

 $\omega_{\rm H}$ is a 3 × 1 vector containing zero-mean Gaussian white noise processes ($\omega_{H} \sim N(0, \mathbf{Q}_{H})$) and the subscript H represents high frequency. The parameter ζ is the relative damping ratio of the motions, and was set as 0.1. The parameter ω_{0} represents the high frequency (wave-induced) motions' peak frequency.

The measured signals **z** are given by:

$$\mathbf{z} = \begin{pmatrix} X_L + X_H + \nu_X \\ Y_L + Y_H + \nu_Y \\ \psi_L + \psi_H + \nu_\psi \end{pmatrix}$$
(7)

where $\mathbf{v} = \begin{bmatrix} v_X & v_Y & v_{\psi} \end{bmatrix}^T$ is a 3 × 1 vector containing zeromean, Gaussian white noise processes ($\mathbf{v} \sim N(0, \mathbf{R})$).

For the sake of simplicity, the matrices Q_L , Q_H , Q_{FL} and R are considered diagonal in real applications. It should be emphasized that the EKF estimates the components x_H and x_L and also low frequency environmental forces F_E .

The complete model can be written as:

$$\dot{\mathbf{x}} = \mathbf{A}(\mathbf{x})\mathbf{x} + \mathbf{B}\mathbf{F}_{T} + \mathbf{E}\boldsymbol{\omega}$$

$$\mathbf{z} = \mathbf{H}\mathbf{x} + \mathbf{v}$$
(8)

with \mathbf{x} , $\mathbf{\omega}$, $\mathbf{A}(\mathbf{x})$, \mathbf{B} , \mathbf{E} and \mathbf{H} given by the obvious association of Eqs. (4)–(7).

The following discrete version of Eq. (8) is used in the EKF algorithm, Δt being the sampling time:

$$\mathbf{x}[k] = \mathbf{f}(\mathbf{x}[k-1], \mathbf{F}_{\mathbf{T}}[k-1], \boldsymbol{\omega}[k-1])$$

$$\mathbf{z}[k] = \mathbf{H} \cdot \mathbf{x}[k] + \mathbf{v}[k]$$

$$\mathbf{f}(\cdot, \cdot, \cdot) = (\mathbf{A}(\mathbf{x}) \cdot \Delta t + \mathbf{I}) \cdot \mathbf{x}[k-1] + \mathbf{B} \cdot \Delta t \cdot \mathbf{F}_{\mathbf{T}}[k-1]$$

$$+ \mathbf{E} \cdot \Delta t \cdot \boldsymbol{\omega}[k-1].$$
(9)

With the model written in the discrete version (9), a discrete EKF algorithm can be directly applied. Defining $\overline{\mathbf{x}}$ as an a priori estimate, $\hat{\mathbf{x}}$ as an a posteriori estimate of state vector, $\overline{\mathbf{X}}$ and $\hat{\mathbf{X}}$, respectively, as the a priori and a posteriori estimates of error matrix covariance, and \mathbf{K} as the Kalman gain matrix, the discrete EKF is given by:

$$\overline{\mathbf{x}}[k+1] = \mathbf{f}(\hat{\mathbf{x}}[k], \mathbf{F_T}[k], 0)$$

$$\overline{\mathbf{X}}[k+1] = \mathbf{\Phi} \cdot \hat{\mathbf{X}}[k] \cdot \mathbf{\Phi}^T + \mathbf{\Gamma} \cdot \mathbf{Q} \cdot \mathbf{\Gamma}^T$$
 (Prediction) (10)

with
$$\Phi = \partial \mathbf{f}/\partial \mathbf{x}|_{\mathbf{x} = \hat{\mathbf{x}}[k]}$$
; $\Gamma = \mathbf{E} \cdot \Delta t$; $\mathbf{Q} = \text{diag}(\mathbf{Q}_{\mathbf{L}} \quad \mathbf{Q}_{\mathbf{H}} \quad \mathbf{Q}_{\mathbf{FL}})$

$$\mathbf{K}[k] = \overline{\mathbf{X}}[k] \cdot \mathbf{H}^{T} \cdot (\mathbf{H} \cdot \overline{\mathbf{X}}[k] \cdot \mathbf{H}^{T} + \mathbf{R})^{-1}$$

$$\hat{\mathbf{x}}[k] = \overline{\mathbf{x}}[k] + \mathbf{K}[k] \cdot \varepsilon[k]$$
 (Correction)
$$\hat{\mathbf{X}}[k] = (I - \mathbf{K}[k] \cdot \mathbf{H}) \cdot \overline{\mathbf{X}}[k]$$

where $\varepsilon[k] = (\mathbf{z}[k] - \mathbf{H} \cdot \overline{\mathbf{x}}[k])$ is the innovation term.

3.2. Controller

The controller most widely used in DP systems is composed of three terms. There is a feedforward wind force compensator, which utilizes the wind speed and direction measured by an anemometer and a simplified model for the estimation of the forces acting on the vessel. Such forces are directly compensated by the controller, and they are counteracted before causing a positioning error.

There is also a Proportional–Derivative feedback controller, which compares the set-points with the estimated positions and heading $\hat{\mathbf{x}}_L$, and calculates the forces to minimize such a difference.

Finally, the integral action is given by the subtraction, from the control forces, of the low frequency environmental forces $\hat{\mathbf{F}}_E$ that is estimated by the EKF.

Fig. 3 presents a block diagram of the EKF and the controller.

PD control gains are adjusted by pole-placement technique, based on a linear model obtained from Eq. (8) for each direction, namely surge, sway and yaw, assuming they are uncoupled.

3.3. Thrust allocation

The thrust allocation logic is responsible for delivering moment and forces calculated by control module algorithms. Such algorithms are oriented towards fuel consumption minimization. The implemented technique, described by [12], is based on a pseudo-matrix inversion, and minimizes the quadratic summation of delivered thrusts. The resultant thrust vector **T** is given by:

$$\mathbf{T} = (\mathbf{A}^T \mathbf{A})^{-1} \mathbf{A}^T \mathbf{F_T}$$
 (12)

where $\mathbf{F_T} = (F_{1T}, F_{2T}, F_{6T})^T$ represents the demanded control forces and moment, and matrix A is given in Box I, being $c_i = \cos(\alpha_{iP})$ e $s_i = \sin(\alpha_{iP})$, α_{iP} the orientation angle when using fixed propellers, and x_i the propeller position according to an orthogonal reference frame fixed to the vessel. The vector \mathbf{T} contains surge and sway force components required in each available propeller, fixed or azimuthing. The required azimuth and thrust are directly obtained from such components.

Some extra features are also included in the allocation algorithm, as follows:

- Reallocation of demanded forces and moment: if the nominal power of a propeller is occasionally exceeded, the difference between the total forces and moment required by the controller and those delivered by the propeller system is calculated, and the difference is reallocated among the nonsaturated propellers;
- Dead zone control: defines prohibited azimuth angles for each propeller, in order to minimize the interference between two propellers or between a propeller and the hull.
- Control of rotation reversal: some propellers are not able to reverse the rotation of their blades or may present a reduced efficiency under reversed rotation. Therefore, the allocation algorithm defines a maximum time during which the rotation can remain reversed until the azimuth angle is rotated by 180° and the propeller rotation re-established.

$$\mathbf{A} = \begin{pmatrix} 1 & \cdot & 1 & 0 & \cdot & 0 & c_{1+n_{\text{azim}}} & \cdot & c_{n_{\text{prop}}} \\ 0 & \cdot & 0 & 1 & \cdot & 1 & s_{1+n_{\text{azim}}} & \cdot & s_{n_{\text{prop}}} \\ -x_{2,1P} & \cdot & -x_{2,n_{\text{azim}}} p & x_{1,1P} & \cdot & x_{1,n_{\text{azim}}} p & -c_{1+n_{\text{azim}}} \cdot x_{2,(1+n_{\text{azim}})} p + s_{1+n_{\text{azim}}} \cdot x_{1,(1+n_{\text{azim}})} p & \cdot & -c_{n_{\text{prop}}} \cdot x_{2,n_{\text{prop}}} p + s_{n_{\text{prop}}} \cdot x_{1,n_{\text{prop}}} p \end{pmatrix}$$

Box I.

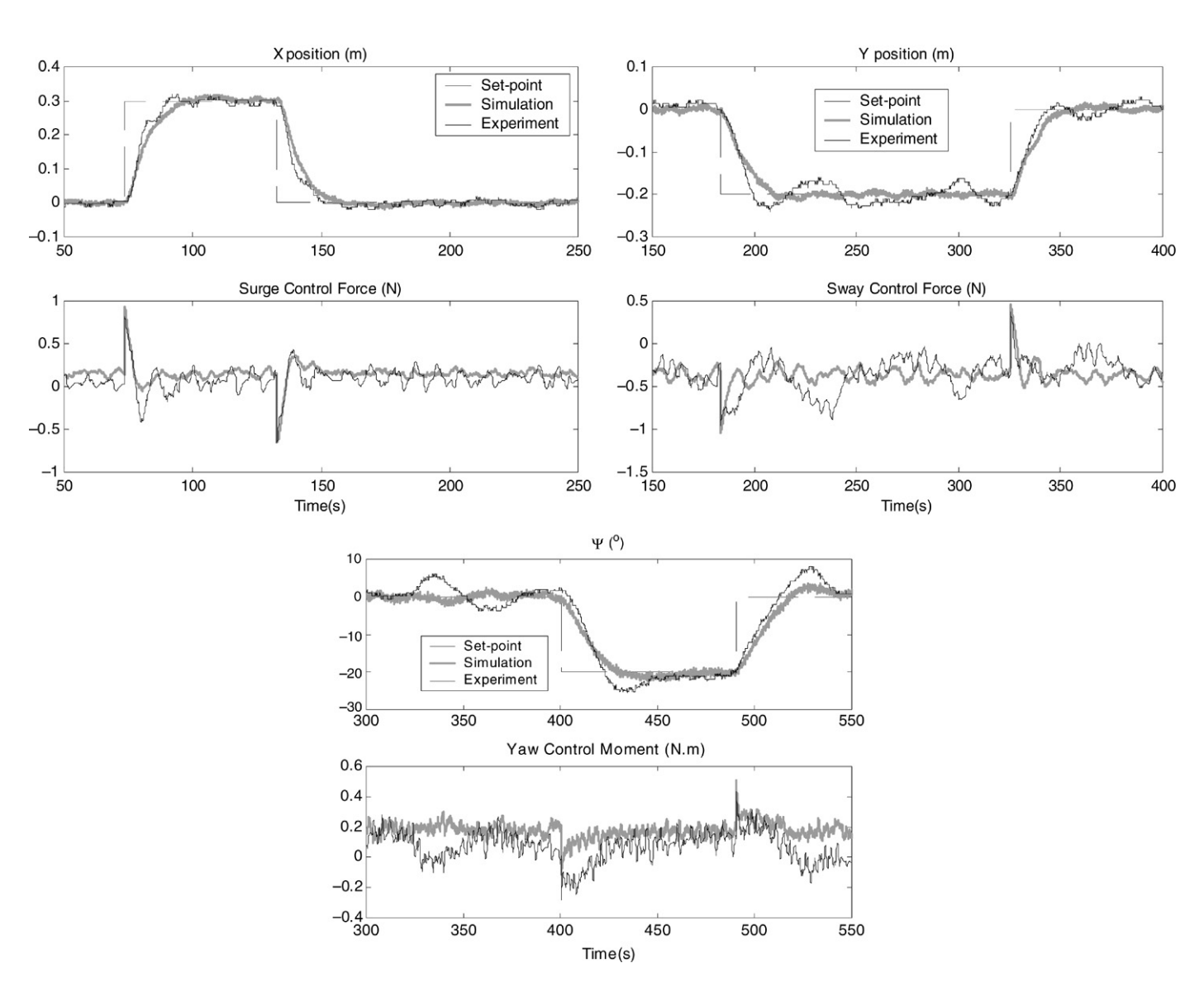


Fig. 12. Full condition, current and wind actions.

 Azimuth filter: it consists of an important way to minimize azimuth oscillation caused by fluctuation of weak demanded control forces. The implemented filter is a classic first-order low-pass one, designed to attenuate frequencies higher than 0.1 Hz.

3.4. Propeller models

The simulator includes models for controllable pitch propellers (cpp) and for fixed pitch propellers (fpp). The model takes into account their characteristic curves, and is able to estimate real power consumption and delivered thrust.

For both types of propellers, the torque (Q_{prop}) and thrust (T_{prop}) are defined accordingly by functions K_T and K_Q as:

$$K_{T}(P/D_{P}, J_{0}) = \frac{T_{\text{prop}}}{\rho |n_{P}|n_{P}D_{P}^{4}};$$

$$K_{Q}(P/D_{P}, J_{0}) = \frac{Q_{\text{prop}}}{\rho |n_{P}|n_{P}D_{P}^{5}};$$
(13)

where n_p is rotation (in rps), D_P is propeller diameter, and ρ is water density. Functions K_T and K_Q are obtained experimentally, and are dependent on blade pitch to propeller diameter ratio (P/D_p) and advance coefficient $(J_0 =$

Table 1 Tanker model properties

	Fully loaded	Ballasted condition			
Mass (kg)	52.5	30.5			
Mom. Inertia (kg m ²)	4.63	5.18			
Length (mm)	1780				
Beam (mm)	290				
Draft (mm)	120	80			

 V_P/n_PD_P), with V_P the inlet water velocity. In the simulator, functions K_T and K_Q are given in either tabular or polynomial form.

For fpp propellers, dynamics of rotating parts are also simulated, accounting for the delay between the control command and the propeller response due to the inertia of the system. Furthermore, for cpp propellers, a maximum pitch variation rate is defined in order to simulate the governor mechanism responsible for the pitch variation.

4. Experimental set-up

In order to make preliminary validations of simulation results, a DPS experiment was implemented in the towing tank of the Department of Naval Architecture and Ocean Engineering.

The tank size is 1.5 m deep, 5 m wide and 21 m long. A reduced scale model of a shuttle tanker was built, with a scale factor $\lambda = 150$. Main dimensions and mass properties of the vessel, in two loading conditions, are given in Table 1.

The actuators of the model of the tanker are 2 tunnel thrusters (a bow and a stern thruster) and the main propeller (see Fig. 4).

The maximum thrusts delivered by the main propeller and tunnel thrusters are about 5.0 N and 0.4 N, respectively. Converting the maximum thrusts to real scale, one obtains 16 900 kN and 1350 kN respectively. Such values are higher than those obtained in a typical DP shuttle tanker, in which the main propeller delivers up to 2000 kN, and each tunnel thruster delivers up to 300 kN. However, since the objective of the present experiment is to make comparisons with the simulator results, such differences between the model and the real ship properties are acceptable since the simulations will be done under the same conditions as the model.

The position and heading are measured by an artificial vision system, comprising of a camera and an image acquisition board. The total resolution of the system is 320×280 pixels, and the monitoring area dimension is approximately 6 m \times 5 m. The resulting resolution of the system is approximately 17 mm. A simplified method to correct the distortion introduced by the lens is also implemented [13]. Two LEDs installed close to the bow and close to the stern are tracked and their positions evaluated. With such an information the software is able to evaluate the midsection position and heading of the vessel. The maximum measurement error due to the resolution is 8.5 mm for the midsection position and 1° for the heading angle.

All numerical calculations are carried out by a Pentium III 800 MHz computer, with a time-step of 0.1 s. The commands to the motors are sent to the ship model by a radio communication module. The control, filter and allocation algorithm is implemented using Matlab/Simulink, including a special block that imposes the simulation to be executed in real-time [14]. A diagram of the experimental set-up is shown in Fig. 5.

Since the ship is equipped only with 3 propellers, the allocation algorithm described in Section 3.3 can be simplified to an algebraic system. Once the surge and sway demanded forces (F_x and F_y respectively) and the demanded moment (F_z) are calculated, the thrust of each propeller can be determined by:

$$\begin{pmatrix} F_1 \\ F_2 \\ F_3 \end{pmatrix} = \begin{pmatrix} 1 & 0 & 0 \\ 0 & 0.5 & -1 \\ 0 & 0.5 & 1 \end{pmatrix} \begin{pmatrix} F_x \\ F_y \\ F_z \end{pmatrix} \tag{14}$$

since the distance between the tunnel thrusters and the midsection is approximately 0.5 m. F_1 is the thrust of the main propeller and F_2 and F_3 are, respectively, thrust of the bow and stern propellers.

The propeller model developed in Section 3.4 is not used in the present experiments and simulations, due to experimental restrictions. Instead of using the thrust coefficients, an experimental arrangement was used to determine the relation between the thrust in each propeller and the command imposed to the motor, using a load cell. The motors are controlled by PWM (pulse width modulation), and the command varies from 0% to 100%. So, after the calculation of F_1 , F_2 and F_3 , the command to the motors can be calculated using such curves. The curve obtained for the main propeller is shown in Fig. 6.

The dead zone is caused by friction and mechanical misalignments of the propeller parts. Furthermore, tunnel thrusters present an even larger dead zone that covers approximately 50% of the command action. This fact may cause unpredictable behavior in propeller action, since the dead zone is highly sensitive to temperature, small displacements of the hull, lubricant, etc.

5. Results and comparisons

The experiments were carried out for two loading conditions (full and ballasted). Fig. 7 shows the ballasted model during an experiment.

Three environmental conditions were considered. In the first condition, no environmental agents were active over the ship. In the second condition, a 0.08 m/s current was imposed on the ship (equivalent to 1 m/s current in real scale), and in the third condition, a wind of approximately 2.4 m/s was simultaneously imposed (Fig. 8).

The current is generated by a tube, mounted transversely in the tank, with several orifices along its length. The wind is generated by a conventional fan. Although such simple apparatus does not guarantee a constant velocity of the environmental actions, the purpose here is only to perform a qualitative evaluation of their effects.

Table 2
PD controller: proportional gains (P) and derivative gains (D)

Condition	Px (N/m)	Py (N/m)	Pz (N m/m)	Dx (N/m/m)	Dy (N/m/m)	Dz (N m/m/s)
Full	2.6	3.6	0.9	16.5	22.7	7.5
Ballasted	1.6	2.2	1.0	9.9	13.6	8.4

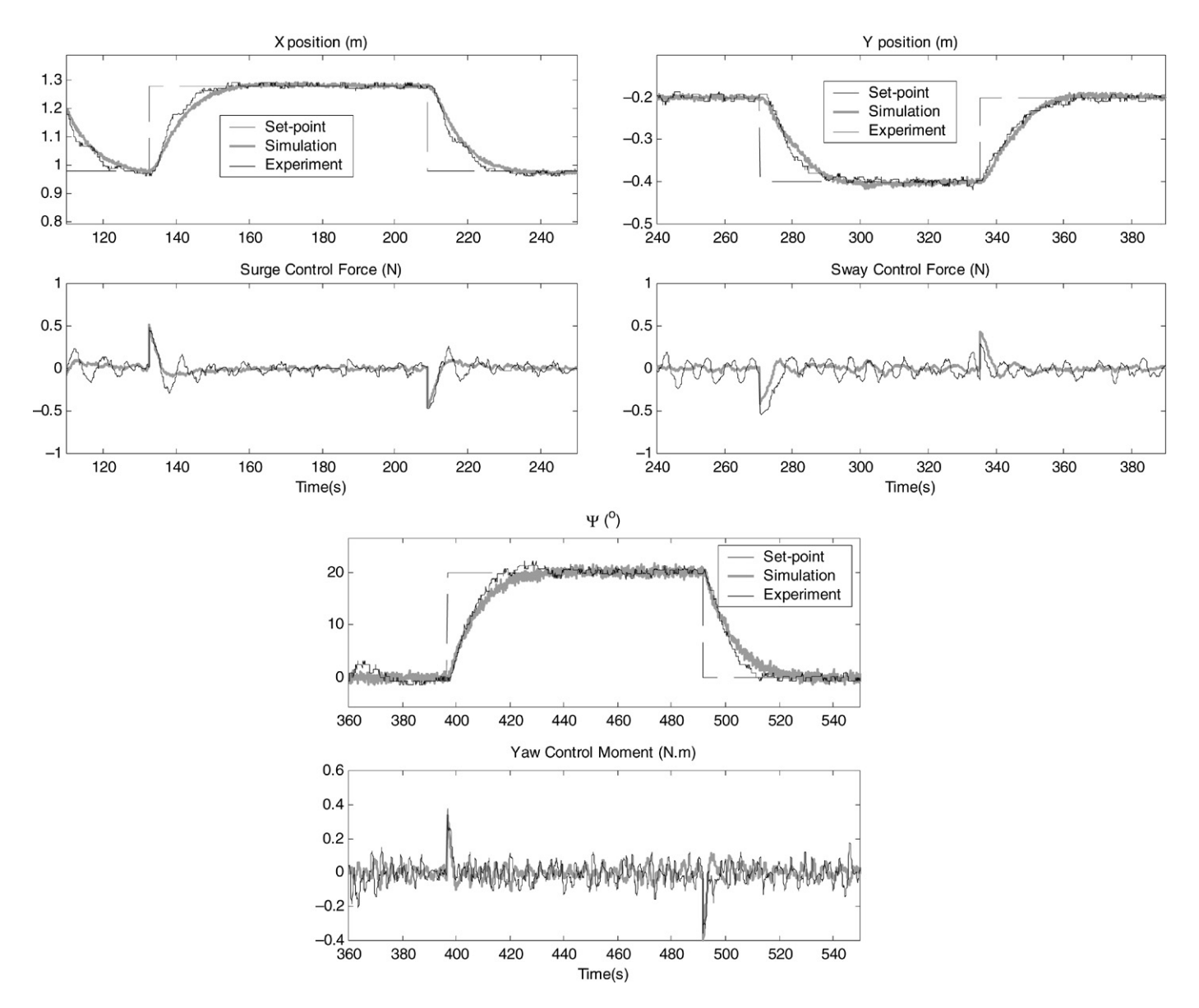


Fig. 13. Ballasted condition, no environmental action.

The PD controller gains used in the simulation and in the experiment are given in Table 2. They were obtained by a pole-placement technique, considering a linearized model of low-frequency motions of the vessels.

The EKF covariance matrices, for both conditions, are given in Box II.

Matrix \mathbf{R} is related to measurement noise, and can be easily adjusted once the accuracy of the sensors applied in DP System

is known. However, the adjusting process of matrix \mathbf{Q} is more complicated. It usually involves a time-consuming trial and error procedure. In the present work, the simulator was used in the tuning procedure, and qualitative conclusions about the effect of changing each term of the matrixes could be drawn. Some of the conclusions were confirmed by the experiments.

For example, increasing the values of the matrix \mathbf{Q} corresponding to elements of the matrix \mathbf{Q}_H , the estimation of

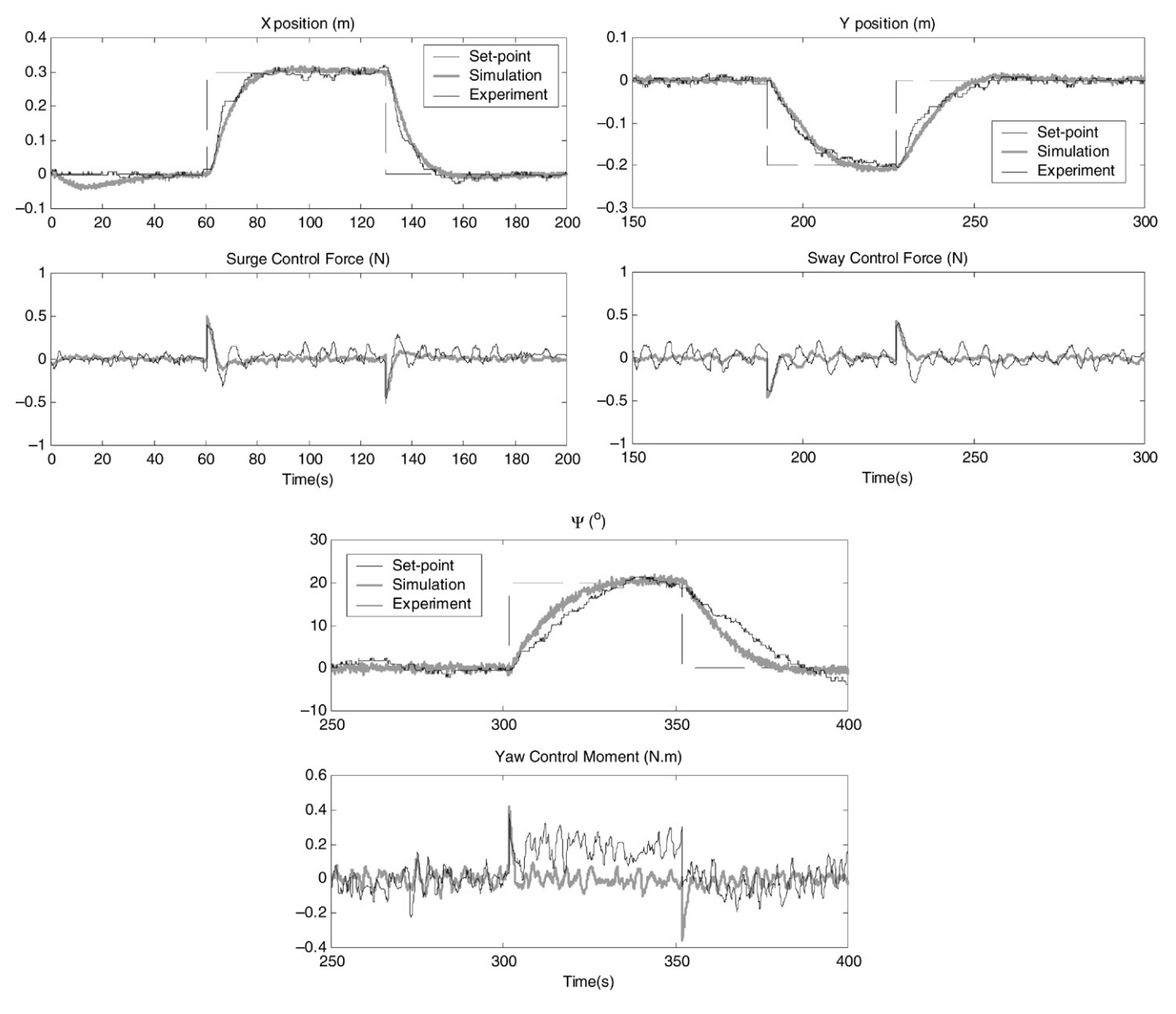


Fig. 14. Ballasted condition, current action.

$$\mathbf{Q} = \text{diag}(0.13 \quad 9 \times 10^{-4} \quad 1.8 \times 10^{-2} \quad 2.2 \times 10^{-3} \quad 2.2 \times 10^{-3} \quad 2.6 \times 10^{-2} \quad 2.1 \times 10^{-3} \quad 1.1 \times 10^{-2} \quad 5.2 \times 10^{-4})$$

$$\mathbf{R} = \text{diag} \left(4 \times 10^{-4} \quad 4 \times 10^{-4} \quad 0.15\right)$$

Box II.

the low frequency motion presents a higher time delay when compared to the real motion, with a stronger attenuation of the high frequency components. The reason for this degradation is that the high frequency model (6) used in the Kalman Filter is more strongly excited, "absorbing" part of the signal energy that should appear in the low frequency model (4). In such a case, the position and heading errors increased, due to the increased time delay.

The reverse occurs with the decreasing of the values of the elements of \mathbf{Q}_H or, analogously, if the values of the elements

of \mathbf{Q}_L are increased. In this case, the low frequency time delay and the attenuation of the high frequency components would decrease. The low frequency model (4) used in the Kalman Filter would 'absorb' high frequency components that should appear in \mathbf{x}_H . The consequence is a very oscillatory control action, due to a poor performance of the control filter.

The added masses, damping, current and wind coefficients used in the simulation were based on a similar vessel, a typical DP shuttle tanker with main dimensions close to the model.

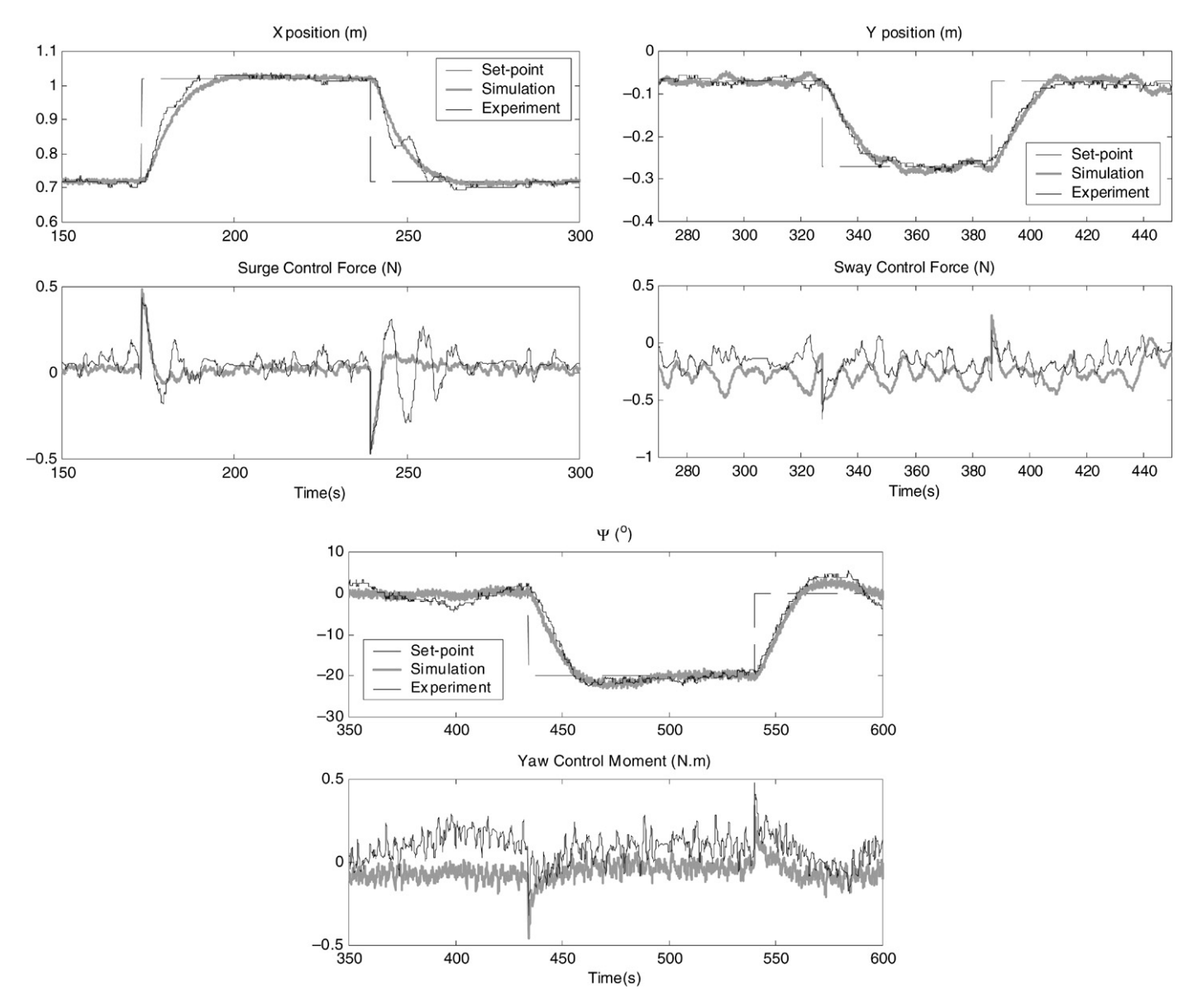


Fig. 15. Ballasted condition, current and wind actions.

As there was no anemometer available in the experiments, the wind-feedforward control was not enabled, in either the simulation or the experiment. White-noise was imposed on the simulation in order to represent the measurement noise of the experiment.

Fig. 9 shows a comparison of the experiment and simulation results, for the fully loaded condition under no environmental action. In all experiments, a 0.3 m step was imposed to the surge set-point, and was retuned after the stabilization. The same kind of motion was imposed on the sway direction (with a step of 0.2 m) and on the yaw (with a step angle of 20°).

Taking into account the simplicity of the experimental setup, the results show quite a good overall agreement between the experimental and the simulation results. In fact, horizontal motions are very well predicted by the simulation. A slightly higher overshoot in the experimental yaw motion may be explained by differences in the proper and added yaw inertia considered in the simulation, as well as in the damping coefficient.

During the set-point changes, the simulation and experimental control forces are very similar, which indicates that the same control algorithms were in fact used. Higher oscillations are encountered in experimental control forces, mainly induced by errors in propeller action (due to the dead zone previously cited) and small delays in control action. Fig. 10 shows the spectra of surge control forces, and the higher oscillations of experimental forces are confirmed, in the range of 0.5–0.8 rad/s (equivalent to a period of 7.8–12.5 s). Such oscillations can be clearly noticed in the time series of the force.

The same conclusions can be drawn from the experiments with current action, shown in Fig. 11. Again, surge and sway motions are very well recovered by the simulation, while larger discrepancies are found in yaw motion during the first set-point

change, which may be explained by errors in evaluating the current moment.

Concerning the actions of the current and wind, Fig. 12 shows that the sway motion observed in the experiment presents larger oscillations, which can be explained by the inconstancy of the wind speed.

In the ballasted condition with absence of the environmental action (see Fig. 13), the comparisons between experiment and simulation are quite good for all motions.

Under the action of current (see Fig. 14) one can notice a large discrepancy between the experimental and simulated yaw moment, while the ship is not aligned with the current. A possible explanation may come from errors in the estimation of the moment delivered by the propellers in the experiment. Such estimation is done by the curves exposed in Fig. 6, which were obtained for the fully loaded ship. In the ballasted case, however, the propellers are closer to the water surface, and a decrease in its efficiency may occur.

Finally, Fig. 15 presents the ballasted ship under the actions of the current and wind. Again, the ship horizontal motion is very well recovered by the simulation.

6. Conclusions

The present paper described two facilities that can be used to analyze, design and predict the performance of DPS aided offshore operations.

The simulator comprises models for main DPS sub-systems, namely control logic, filtering, thrust allocation and propulsion. It enables the simulation of three DP operations: station keeping, path following, and DP assisted offloading. The conventional control and filtering algorithm was implemented, namely an Extended Kalman Filter cascaded with a 3-axis uncoupled PD controller. The simulator also considers fixed and azimuthing propellers modeling, as well as controllable or fixed pitch propellers. It takes into account their dynamics and time response characteristics. Finally, the thrust allocation algorithm is included, minimizing fuel consumption.

A simple experimental set-up was implemented and used to pre-validate the simulator. Several experiments with a reduced model of a DP tanker with 3 thrusters subjected to current and wind actions were performed. The experimental and simulation results were compared in detail, and shown to be in good agreement, considering the simplicity of the experimental set-up.

Acknowledgments

The first author acknowledges a research grant, no. 02/07946-2, from FAPESP. The authors are grateful to Alessandro de Oliveira Santos, Glenan Assis Lago, Vinicius L.M. Veras, Diego Massola Shimizu, Lázaro Moratelli Junior and Fernando Akihiro Morikawa, students of the University of São Paulo.

References

- [1] Nishimoto K et al. Numerical offshore tank: Development of numerical offshore tank for ultra deep water oil production systems. In: Proceedings of the 22th international conference on offshore mechanics and artic engineering. 2003.
- [2] Balchen JG, et al. A dynamic positioning system based on Kalman filtering and optimal control. Modeling, Identification and Control 1980; 1(3):135-63.
- [3] Tannuri EA, Morishita HM, Veras VLM, Lago GA. Critical analysis of control and filtering algorithms used in real dynamic positioning systems. In: Proceedings 24th international conference on offshore mechanics and arctic engineering. 2005.
- [4] Bray D. Dynamic positioning. The oilfield seamanship series, vol. 9. Oilfield Publications Ltd (OPL); 1998.
- [5] Fossen TI, Strand JP. Passive nonlinear observer design using Lyapunov methods, experimental results with a supply vessel. Automatica 1999; 35(1):3–16.
- [6] Simos AN, Tannuri EA, Pesce CP, Aranha JAP. A quasi-explicit hydrodynamic model for the dynamic analysis of a moored FPSO under current action. Journal of Ship Research 2001;45(4):289–301.
- [7] OCIMF. Predictions of wind and current loads on VLCCs. In: Oil companies international marine forum. 1994.
- [8] Aranha JAP. A formula for wave damping in the drift of a floating body. Journal of Fluid Mechanics 1994;272:147–55.
- [9] Tannuri EA, Bravin TT, Pesce CP. Development of a dynamic positioning system simulator for offshore operations. In: 17th international congress of mechanical engineering. 2003.
- [10] Nishimoto K, Fucatu CH, Masetti IQ. Dynasim—A time domain simulator of anchored FPSO. In: Proceedings of the 20th international conference on offshore mechanics and artic engineering. 2001.
- [11] Morishita HM, Bolognani Y. Dynamics and control of a two-body floating system under realistic environmental loads. Applied Mathematics and Computation 2005;164:573–90.
- [12] Sørdalen OJ. Optimal thrust allocation for marine vessels. Control Engineering Practice 1997;5(9):1223–31.
- [13] Gribbon KT, Johnston CT, Bailey DG. A Real-time FPGA implementation of a barrel distortion correction algorithm with bilinear interpolation. In: Proceedings of image and vision computing New Zealand. 2003. p. 408–13.
- [14] Daga L. Leonardo Daga's warehouse, Available in http://digilander.libero.it/LeoDaga/index.htm. [accessed: 28. 02. 06].